European Journal of Orthodontics 23 (2001) 647–662 © 2001 European Orthodontic Society

Endothelin-1 expression in the microvasculature of normal and 3-hour continuously loaded rat molar periodontal ligament

Milton R. Sims
Microcirculation and Lymphology Laboratory, Flinders University of South Australia and Orthodontic Unit, University of Adelaide, South Australia

SUMMARY Endothelin-1 (ET-1) distribution is described in the microvascular bed (MVB) of normal rat molar periodontal ligament (PDL). Five male Sprague–Dawley rats, aged 90 days, were anaesthetized and an external pressure of 100 ± 20 g, maintained for 3 hours, was transmitted occlusally to randomly allocated left or right molars. The controls were the contralateral molars.

Rats were perfused for 5 minutes with 5 per cent paraformaldehyde, and the mandibles post-fixed and stored in 30 per cent sucrose. Sagittal, undemineralized, mandibular jaw sections, ~150 μm thick, were immunolabelled with ET-1 and alpha-smooth muscle actin (α-SMA) primary antibodies, and IgG/CY5 and IgG/CY3 secondary antibodies, respectively. Serial images were captured with a Bio-Rad MRC-1000UV confocal laser scanning microscope (CLSM).

In the control PDL, the ET-1 immunolabelling occurred sporadically in all categories of PDL blood vessels. ET-1 showed a punctate distribution within endothelial cells, producing longitudinal and circumferential pan-endothelial labelling. Immunoreactivity to the ET-1 antibody occurred at or adjacent to vessel branching sites, and affected blood vessels with and lacking α-SMA immunolabelling.

Treatment effects on ET-1 immunofluorescence were analysed for vascular endothelium, socket bone surface cells, cementum surface cells and PDL background in the cervical, inter-radicular and apical regions. Significant ($P < 0.05$) region by treatment interactions occurred for the endothelium and bone. Cementum showed a significant ($P < 0.05$) region effect and a significant ($P < 0.05$) treatment effect. However, the region by treatment interaction was not significant. Background immunofluorescence showed significant ($P < 0.05$) region by treatment effects for the endothelium and bone. ET-1 activity is the default state for normal PDL vascular endothelium.

Introduction

Endothelin-1 (ET-1) is the major isoform of a family of three different isopeptides widely distributed in the tissues of animals and humans. Endothelins are differentially expressed in a tissue specific manner (Brooks, 1997). Depending on the species, particular tissues may contain one or more of these distinct peptides or their receptors (Horowitz *et al*., 1995). The endothelins are synthesized by the vascular endothelial cells of arteries and veins, and ET-1 is reported to be one of the most potent vasoconstrictors known (Yanagisawa *et al*., 1988; Ames *et al*., 1999) producing rapid and long lasting changes in cell function (Gray, 1995). The ET-1 peptide has many functions including the control of vascular smooth muscle tone, influencing tissue remodelling, stimulating cellular hypertrophy and hyperplasia, matrix synthesis, chemokinesis, and the release of growth factors and adhesion molecules (Wang *et al*., 1996). This isoform is also important in craniofacial development (Ong, 1996).

In dental tissues, ET-1 has been described in the blood vessel endothelium of normal and inflamed human dental pulp (Casasco *et al*., 1992) and the infused canine pulp (Gilbert *et al*., 1992). Subsequently, Shiohama *et al*. (1995) demonstrated the presence of ET-1 in osteoclasts and reported a generalized distribution of ET-1 in the periodontal ligament (PDL) of rat molars exposed to continuous, bone deforming loads. Although Shiohama *et al*. (1995) stated that ET-1 occurred in the PDL vessel endothelium, the microvascular bed (MVB) associations were not detailed.

The present investigation used undecalcified slices of rat jaw to study the distribution of ET-1 in the blood vessels of the molar PDL and ascertain its relationship to vascular alpha smooth muscle actins (α-SMA) in vessel walls. These associations in normal mandibular molars were compared with the contralateral molars subjected to a 3-hour continuous intrusive load. It was hypothesized that this short-term, occlusal load would produce upregulation of ET-1 in the dental microvasculature.

Materials and methods

This protocol was approved by the Animal Ethics Committee of the University of Adelaide and conformed to the NH&MRC guidelines for animal welfare. Five, 90-day-old, male Sprague–Dawley rats (350 ± 40 g) were sedated with halothane and anaesthetized intraperitoneally with nembutal (60 mg/ml: 0.1 ml/100 g weight). A two-piece stainless steel telescoping frame was placed over the snout and mandible (Sims, 1999). Latex orthodontic elastics attached between the top and bottom halves of the frame produced a closing load of 100 g to the jaws. This load was transmitted to the PDL via a rubber pad randomly assigned to the left or right side and placed occlusally between the molars. The non-loaded side acted as the control. Anaesthesia and loading were maintained for 3 hours and body temperature controlled with an insulating blanket. Following thoracotomy, under surgical anaesthesia, a cannula was then tied into the aorta for perfusion fixation and the inferior vena cava was cut to allow free blood egress. The blood was washed out with buffered saline at a pressure of 200 mm Hg, followed by 5 per cent paraformaldehyde perfusion for 5 minutes. The mandibles were removed, cleaned, and immersion fixed for a further 2 hours in paraformaldehyde and stored in 30 per cent sucrose solution containing 1:10,000 thimerosal (Sigma, Sydney, Australia). Tissue sections ~150 μm thick, were cut through the molar regions in a sagittal orientation using a 200-μm thick, stainless steel, diamond studded disc revolving at slow speed under a stream of cold, double strength, 0.2 M phosphate buffered saline (PBS).

Molar sections were processed for immunostaining in contralateral pairs by dehydration through an ethanol series to 100 per cent and permeablized in DMSO (dimethylsulphoxide). After washing with 0.2 M PBS (pH 7.4) for 1 hour, the tissues were blocked with 10 per cent donkey serum in 0.2 M PBS for 2 hours. The slices were then incubated at ~20°C in a humid chamber for 72 hours with the primary antibody (rabbit × human anti-ET-1; IHC 6901, Peninsula Laboratories Inc., San Carlos, CA, USA) at a 1:50 titre in 10 per cent donkey serum in double strength PBS. After washing, the slices were reincubated for 48 hours in secondary antibodies (IgG conjugated donkey × rabbit CY5; Jackson Laboratories, West Grove, PA, USA) diluted 1:50 in double strength PBS antibody diluent. The immunostaining was then repeated using mouse × human α-SMA (MAB-0003; Maxim Biotech Inc., San Francisco, CA, USA) at a 1:50 titre followed by donkey × mouse CY3 (Jackson Laboratories) at 1:50. The slices were washed with 0.2 M PBS and the preparations mounted in 80 per cent buffered glycerol (pH 8.5). Negative control sections were processed simultaneously, omitting primary, and/or secondary antibodies.

Tissues were viewed with a Bio-Rad MRC-1000UV (Bio-Rad, Hemel Hempstead, Herts, UK) confocal laser scanning microscope (CLSM) using a krypton/argon laser. The CY5 label was visualized with excitation of 647/10 nm and emission 680LP nm, and the CY3 with excitation 568/10 nm and emission 605/32 nm. The images were captured as digital files in serial sections with stacked layers to create 3-D reconstructions (Sims, 1999). For all images the fluorescence intensity was kept within the

dynamic range of the camera. Image data were not enhanced post-collection. More sensitive settings of the CLSM were used for recording the control sections than their experimental counterparts. On the other hand, the immunofluorescence of the loaded vessels, hard tissues, and the PDL background was so enhanced that it was necessary to reduce their CLSM settings to minimize image over-saturation.

Statistical analysis

Since statistical data collection required protracted CLSM re-imaging, the data pool was limited to rats number 3 and 4, which had ideal, paired, mid-sagittal sections. The endothelium ET-1 labelling of all vessels was evaluated in a representative, single optical slice from the cervical, inter-radicular and apical regions using 256 levels of signal-to-background ratio based on grey scale intensity-coded readings (Sims, 1999). The ET-1 label was recorded at 10-μm intervals along opposite vessel sides using a 1.5 × 5.0-μm box. Vessel segments 10–15 μm in length were sampled once on each side, vessels 16–25 μm long had two samples per side, vessels 26–35 μm long had three samples, and so on. Corresponding PDL background data were obtained with a 5 × 7.5-μm box at a distance of 5 μm between box centres (Figure 1). The mean endothelium and PDL background ET-1 values were determined for each data pair.

Sixty-six control, and 113 experimental section vessels provided 226 and 306 data pairs, respectively. Bone surface cell immunolabelling along the socket was sampled in the cervical, inter-radicular, and apical regions with 10 equidistant readings along a length of ~200 μm, using an 11 × 17-μm box and an 20 × 30-μm background PDL box centred 30 μm from the bone at right angles to the surface. Corresponding regions for the cementum surface cell immunolabelling were recorded with 10 equidistant readings along ~200 μm using 11 × 17-μm boxes. The PDL background box was centred 30 μm from the cementum box at right angles to the perimeter (Figure 1).

Data were analysed initially as ratios of endothelium, bone surface cell and cementum surface cell ET-1 immunofluorescence to their matched PDL background immunofluorescence. The use of ratio data accorded with customary CLSM practice. The technique applied was the

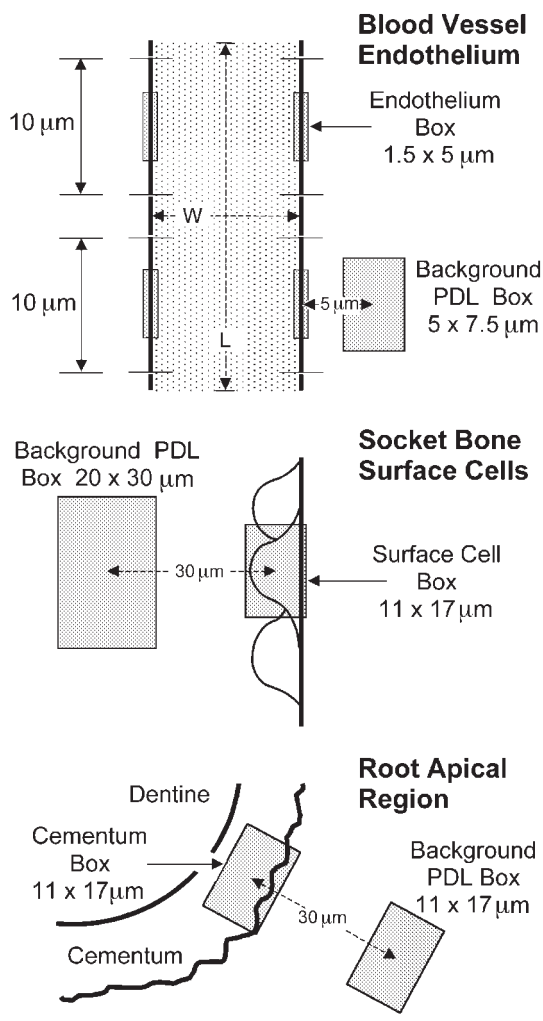

Figure 1 Schematic diagram of the sampling protocol for the immunofluorescence intensity of ET-1 labelling of blood vessel endothelium, bone surface cells and cementum surface cells. The endothelium was recorded at 10-μm intervals on opposite sides using a 1.5 × 5.0-μm box. A 5 × 7.5-μm PDL background box was used at a distance of 5 μm between the box centres. Vessel length and width are designated (L) and (W), respectively. ET-1 labelling of bone socket surface cells and cementum surface cells, was sampled with 10 readings along a length of ~250 μm in the cervical, inter-radicular and apical regions using an 11 × 17-μm box. The PDL background boxes of 11 × 17 μm were centred at right angles 30 μm distant to the bone and cementum boxes.

method of Restricted Maximum Likelihood (Paterson and Thompson, 1971) from within the statistical package Genstat 5, Release 3 (Payne *et al*., 1993). The effects of the teeth and vessels were considered random effects, and the treatment and regions as fixed effects.

Because of the marked ET-1 upregulation in the experimental PDL background, the CLSM resetting resulted in ratio bias to the data and decreased the real extent of ET-1 upregulation. Therefore, it proved necessary to conduct additional analyses of the individual observed data sets for the endothelium, bone surface cells, and cementum surface cells, and also an analysis of their specific PDL background values. For the latter analyses, random errors were assumed to be present.

A log transformation of the data was required to ensure that the residuals from the measurements were normally distributed. In all cases, the among teeth variance component was estimated as negative and, hence, this term was removed from the model. In effect, this meant that the experimental units were the vessels in the case of the endothelium, and the individual measurements in the case of the bone and cementum.

Results

The five consecutively treated animals showed comparable immunohistochemistry patterns with ET-1 and α-SMA labelling in the control PDL, and the experimental sections. Counting showed ET-1 labelling in 40 per cent of control and 41 per cent of experimental blood vessels. Venous vessel profiles were classified by their diameter and wall thickness (Tang and Sims, 1992). Arterial vessels with an external diameter <10 μm were classed as arterial capillaries (AC); those with an external diameter of 10 μm or more were designated terminal arterioles (TA). Control PDL showed positive ET-1 immunoreactivity at scattered sites throughout the MVB in some venous capillaries (VC) with luminal diameters ranging from 3 to < 8 μm and post-capillary-sized venules (PCV) from 8 to 30 μm. Arterial vessels labelled with α-SMA varied from 4 to 65 μm in external diameter. The majority

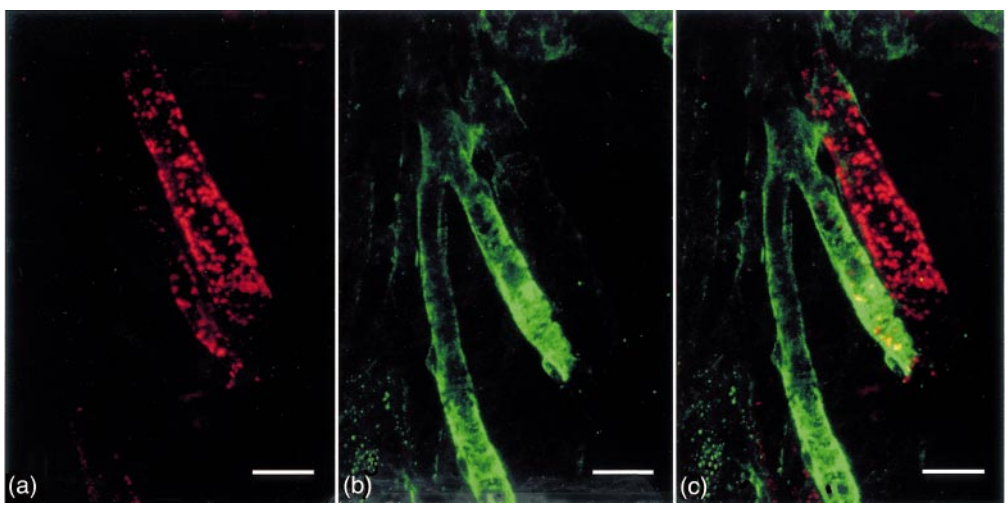

Figure 2 (a) ET-1 immunoreactivity visualized with a CY5 fluorescent secondary antibody label imaged in the red channel. The ET-1 is distributed in a punctate pattern in a PCV and portion of an adjacent TA. Stack of 11 images at 2-μm intervals. Control PDL below the mesial alveolar crest and adjacent to the socket wall. (b) The matching image stack for Figure 2a, showing immunolabelling with α-SMA in a branching TA, using a CY3 fluorescent label imaged in the green channel. (c) Merged image of Figures 2a and b. The ET-1 label defines a PCV endothelial tube devoid of α-SMA investment. The adjacent branch of a TA shows some ET-1 labelling in its endothelium, whereas the lateral TA branch is labelled only with α-SMA antibody. Scale bar = 20 μm.

of vessels showing ET-1 and α-SMA immunoreactivity were located in the PDL middle and bone circumferential thirds. There were different patterns of vascular immunoreactivity. In the cervical region and throughout the PDL, some VC or PCV vessel segments were labelled only with ET-1 (Figure 2a). AC and TA were demarcated solely by α-SMA, or showed both ET-1 and α-SMA immunofluorescence in their walls (Figures 2b,c).

The asymmetrical distribution of vessel ET-1 immunolabelling, both circumferentially and longitudinally, was a consistent feature. Endothelial wall ET-1 immunoreactivity occurred as punctate intracellular elements having a granular appearance (Figure 2c). In control endothelium their size varied from barely visible dots to granules ~2 μm across. Their distribution could extend over large areas of endothelium in vessels with or without smooth muscle.

In the control sections, groups of TA were observed coursing across the PDL from the apical alveolar bone to the molar root canals. These vessels were strongly labelled by the α-SMA antibody, but showed no evidence of endothelium immunoreactivity to the ET-1 label (Figure 3). At the branching sites of control TA, the α-SMA signal frequently identified marked constriction regions with or without the presence of ET-1 reactivity (Figure 4). The distribution of ET-1 also occurred in punctate or continuous patterns where α-SMA labelled TA of 14–30 μm at branching sites.

Experimental molar loading resulted in upregulation of ET-1 immunoreactivity. Loaded sections showed twice the number of experimental vessels compared with control PDL. This change was most evident in the apical and inter-radicular zones, and in proximity to the socket walls. Where ET-1 was the only detectable label, it was located in VC and PCV. In the loaded endothelium, the punctate ET-1 pattern was present as discrete intracellular granules with profiles of granules up to 4.5 × 3.0-μm in size (Figure 5).

Loaded PDL showed microvascular ET-1 distribution patterns similar to those in control tissue with asymmetrical immunolabelling. Many of the PCV, devoid of immunolabelling along their major diameter, revealed an abrupt and intense ET-1 upregulation around a bifurcation site or in the endothelium of a smaller tributory branch (Figure 6). Some AC and TA with external diameters ranging from 10 to 16 μm showed strong ET-1 upregulation.

The vascular inconsistency in the association between ET-1 and α-SMA immunolabelling was

Figure 3 A group of arterioles coursing through the apical PDL between the bone and the molar mesial root canal reveal only α-SMA immunolabelling, with no evidence of ET-1 antibody label. Control PDL. Merged stack of six images spaced at 10 μm. Scale bar = 20 μm.

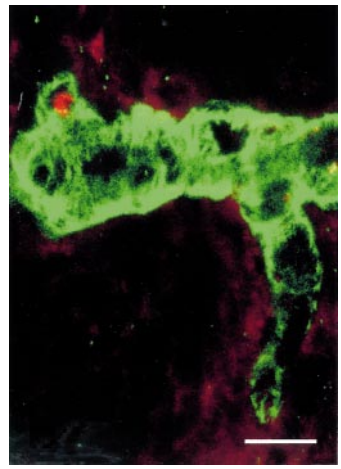

Figure 4 Tangential slice through an arteriole defined with α-SMA antibody. The two branches show constrictions at their origin and an ET-1 label at one branch. Merged stack of 11 optical slices 2 μm apart. Control PDL. Scale bar = 20 μm.

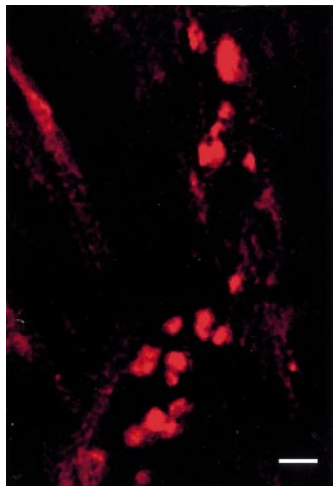

Figure 5 Punctate pattern of ET-1 immunoreactivity in PCV endothelium of loaded PDL. Section labelled with both ET-1 and α-SMA primary antibodies and CY5 and CY3 secondary antibodies, respectively. No smooth muscle is evident. Merged stack of seven optical slices at 4-μm intervals. Scale bar = 4 μm.

Figure 6 A PCV double labelled with ET-1 and α-SMA primary antibodies, and CY5, CY3 secondary antibodies. The main segment of the PCV, indicated by the dashed blue lines, lacks any antibody signal. Strong ET-1 up-regulation is present in the lateral vessel branch, but both vessels lack smooth muscle. Single optical slice. Experimental PDL. Scale bar = 10 μm.

exemplified in experimental sections containing long sections of TA demarcated solely by the α-SMA label. Where a branch showed segmental upregulation of ET-1, its red colour image was partly masked by the enveloping green α-SMA label, producing a superimposed yellow image (Figure 7a). When the images of the α-SMA label of the branch were omitted from the full stack, the intensity and extent of the ET-1 upregulation within the branch became evident (Figure 7b).

Where VC, PCV, and TA vessel groups coursed together in loaded PDL the upregulation produced pan-endothelium ET-1 labelling of the PCV and VC. The accompanying TA showed both ET-1 and α-SMA signals (Figure 8). The juxtaposition of similar immunoreactive vessels in control PDL did not reveal any indication of co-localization of the ET-1 and α-SMA (Figure 9). By contrast, in loaded PDL there was evidence of strong ET-1 and α-SMA co-localization where juxtaposition of PCV and TA occurred (Figure 10).

Inter-radicular regions of the PDL showed similar ET-1 and α-SMA responses to those occurring elsewhere. Whereas the normal PDL had an occasional VC and PCV showing ET-1 immunolabelling, and the odd AC and TA (Figure 11a), the experimental inter-radicular PDL demonstrated strong upregulation of ET-1 in the VC and PCV (Figure 11b). Furthermore, many of the clearly demarcated TA exhibited punctate ET-1 labelling of their endothelium.

Experimental apical PDL showed the most marked evidence of ET-1 upregulation. Where the section contained interconnecting arcades of blood vessels, it revealed ET-1 in VC and PCV endothelium devoid of α-SMA immunoreactivity (Figures 12a,b). The majority of vessels affected were PCV from 11 to 16 μm in diameter.

Arterial vessels reacting with α-SMA antibodies were present throughout the control and experimental PDL. The α-SMA immunofluorescence was present in two principal patterns; a continuous investment surrounding a vessel, or an irregular and partial encirclement of blood vessel endothelium. Many vessel segments were labelled solely for α-SMA (Figures 2c and 3), whereas others displayed a varying, but simultaneous, expression of ET-1 labelled endothelium (Figures 2a,c). In control apical PDL the large

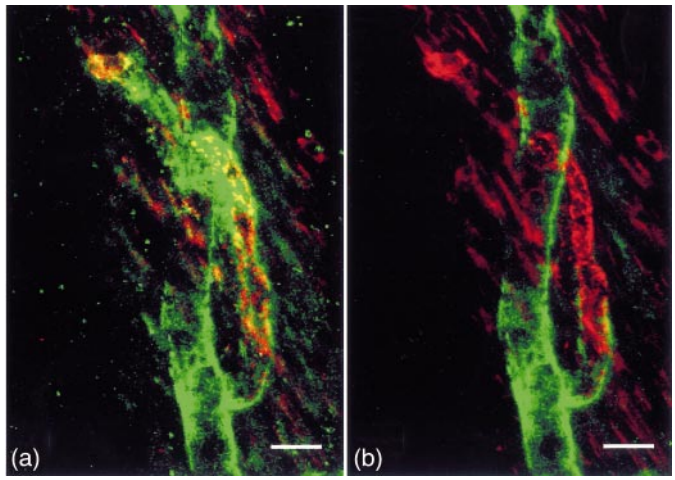

Figure 7 (a) TA segment in experimental PDL depicting the heterogeneous nature of ET-1 upregulation within the microvasculature. The TA and its branch are identified with α-SMA antibody. There is no ET-1 signal in the main TA segment. The branch has an irregular path, curving below the main vessel and coursing laterally to turn upwards again at its extremity. Close to its origin from the main vessel, the branch shows slight ET-1 labelling which becomes significantly upregulated in the middle section and then reappears at the extremity. Merged stack of 26 optical slices spaced at 4 μm. (b) The same TA segment depicted in Figure 7a with the ET-1 immunolabel throughout the stack of 26 optical slices. However, the α-SMA antibody label for the arteriole branch has been omitted from slices 17 to 26 to reveal the full extent of ET-1 upregulation. Non-specific background upregulation is present within the PDL. Scale bar = 20 μm.

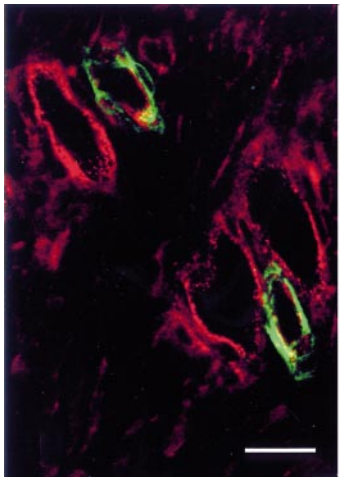

Figure 8 TA profiles labelled with both ET-1 and α-SMA antibodies are shown adjacent to PCV and VC profiles with upregulation of their ET-1 immunolabelling. Cervical region adjacent to the alveolar wall. Single optical slice. Experimental PDL. Scale bar = 20 μm.

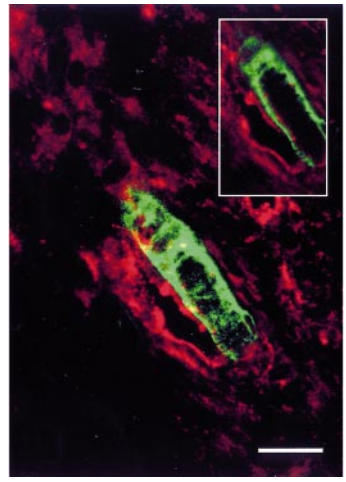

Figure 9 Immunolabelling in control PDL reveals a PCV with ET-1 and an adjacent arteriole with α-SMA. At the juxtaposed abluminal wall boundaries there is close proximity of PCV endothelial ET-1 interaction with the smooth muscle of the TA. Merged stack of seven optical slices at 2-μm intervals. Inset is a single optical slice from the stack. Scale bar = 20 μm.

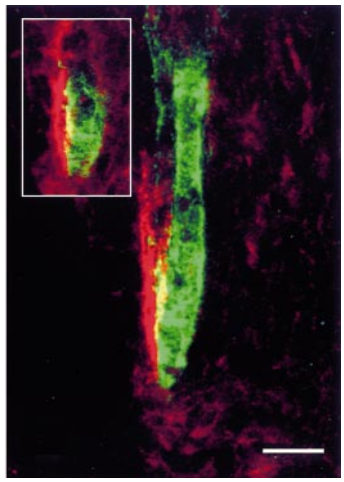

Figure 10 Experimental PDL with a juxtaposed PCV and TA suggesting a possible paracrine relationship between the ET-1 in the PCV endothelium, and the α-SMA of the TA smooth muscle at their adjacent abluminal surfaces. Merged stack of 12 optical slices spaced at 4 μm. Inset is a single slice. Scale bar = 20 μm.

TA from 30 to 35 μm in external diameter showed no evidence of ET-1 immunoreactivity. Similar TA in loaded apical PDL showed slight evidence of ET-1 upregulation. However, some AC and TA, with external diameters ranging from 10 to 16 μm, showed strong ET-1 upregulation throughout the experimental PDL (Figures 2c, 7a,b, 8, 10, 11b, 12b). In control PDL, occasional bone surface cells of the socket wall, the cementum surface cells, and macrophages showed ET-1 immunohistochemical reactivity. These cells were more prominent in the coronal third of the PDL than the apical zone. At isolated sites around the root, particularly at the apex, small groups or cords of cementum surface cells showed a strong ET-1 label (Figure 12a).

Experimental PDL demonstrated strong ET-1 upregulation of bone surface cells on the socket wall and cementum surface cells on the roots, particularly at sites where bone or cementum irregularities protruded into the PDL. Furthermore, the general PDL cell population and the mucopolysaccharide ground substance showed a characteristic, but non-specific, increase in ET-1 background immunoreactivity in the cervical, inter-radicular and apical regions (Figures 7a,b, 11b, 12b). As a result, the strong upregulation of ET-1 in the VC and PCV appeared to be relatively diminished against the strongly affected background reaction.

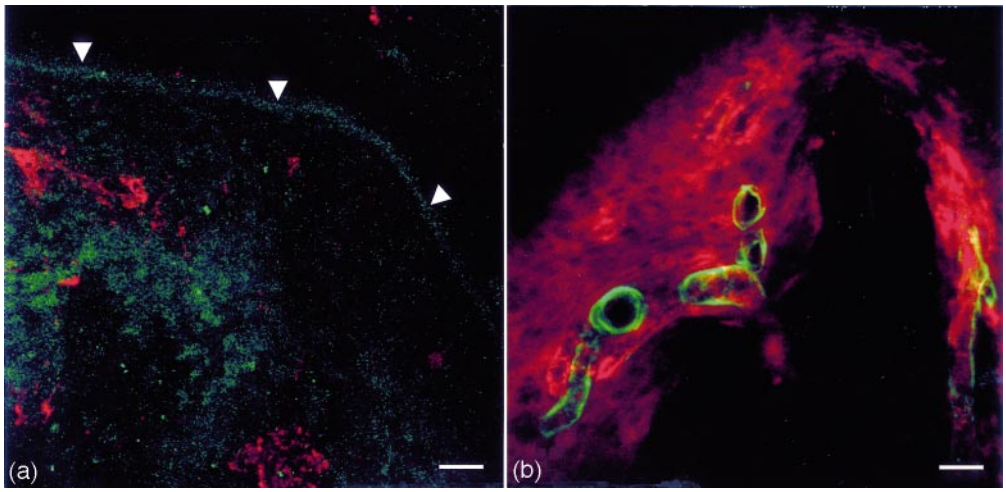

Figure 11 (a) Inter-radicular control PDL labelled for α-SMA and ET-1. Isolated PCV and VC are present. This PDL section lacked arterioles. Non-specific background staining of the PDL is absent. The gamma value of this image was increased to reveal the cementum outline indicated with arrowheads. Merged stack of 14 optical slices spaced at 4 μm. (b) Experimental inter-radicular PDL from the contralateral molar in Figure 11a. One large TA profile has ET-1 upregulation in the endothelium, whereas other TA profiles lack this feature. There is non-specific upregulation of ET-1 immunolabelling in the PDL. Merged stack of three images spaced at 4 μm. Scale bar = 20 μm.

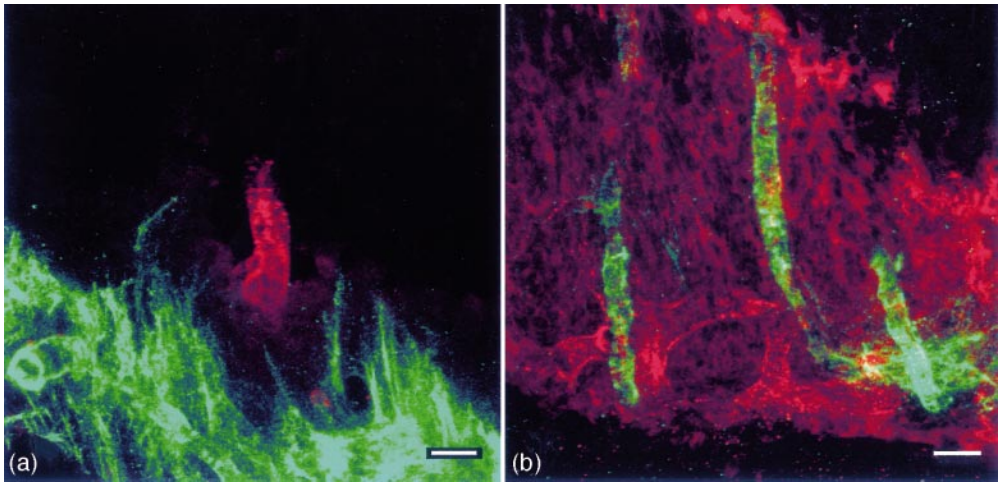

Figure 12 (a) Apical control PDL. What appears to be a solitary vessel demarcated with ET-1 antibody is actually a small cord of upregulated cementum surface cells. Tangentially-sectioned TA and collecting venules above the bone boundary are labelled with α-SMA. Merged stack of nine images spaced at 2 μm. (b) Experimental apical compression region from the contralateral molar PDL of the animal in Figure 12a. An arcade of interconnecting PCV with upregulated endothelial ET-1 labelling is present. There is ET-1 immunolabelling in the endothelium of the arterioles. Upregulation has occurred in tooth cementum surface cells. Merged stack of 15 optical slices separation at 2 μm. Scale bar = 20 μm.

Statistical findings

A feature of the overall analysis was that the between-rat differences for equivalent regions in both control and treatment sections were very small.

Analysis of ratio data. The results of the Wald test are given in Table 1. Effects indicated by an asterisk are considered significant at the $P < 0.05$ level.

The Wald statistics were very large, and clearly indicated some effect for endothelium, bone and cementum. There was a very clear region, and region by treatment interaction for the endothelium ($P < 0.05$) and for the bone surface cells ($P < 0.05$). Endothelium showed a significant ($P < 0.05$) region effect. In the cementum surface cells, there was no evidence of a treatment effect, although there was a significant ($P < 0.05$) region effect. Ratio data of background immunofluorescence for endothelium, bone surface cells and cementum surface cells are summarized as means in Table 2 and Figure 13a–c.

Analysis of observed endothelium, bone cell and cementum cell data. Wald test for the effects of region and treatment on ET-1 immunofluorescence in endothelium, bone surface cells, and cementum surface cells, after removing the among tooth variance component, are given in Table 3.

Table 1 Wald test for ET-1 upregulation: ratio data.

Term	Wald statistic	d.f.	Endothelium	Bone	Cementum
Region		2	10.0*	44.9*	31.5*
Treatment		1	1.3	19.4	0.4
Region by treatment		2	26.3*	32.9*	1.7

*$P < 0.05$.

Table 2 Control and loaded means for ET-1: ratio data.

Treatment	Endothelium		Bone		Cementum	
	Control	Loaded	Control	Loaded	Control	Loaded
Region						
Cervical	1.557	1.299	0.597	1.601	0.801	1.106
Inter-radicular	1.727	1.789	1.384	1.455	1.100	0.948
Apex	1.356	2.015	1.368	1.992	1.453	1.856

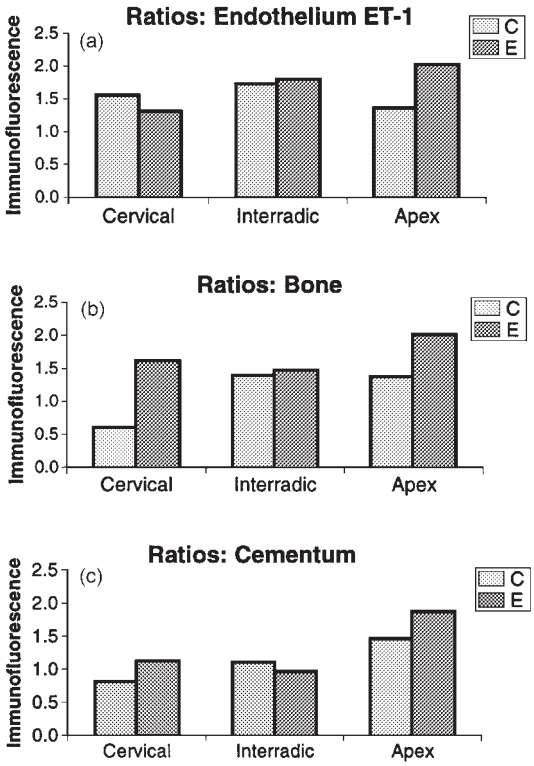

Figure 13 (a) Mean ratios for the regional immunofluorescence intensity level of vessel endothelium ET-1 against the matching PDL background boxes in control and loaded sections. (b) Bone socket surface cell ET-1 against the matching PDL background boxes in control and loaded sections. (c) Cementum cell ET-1 against the matching PDL background boxes in control and loaded sections. C = control, E = experimental.

Significant ($P < 0.05$) interactions were indicated between the treatment and the region in ET-1 immunofluorescence for both the endothelium and bone surface cells. However, there was little interaction between the treatment and region for the cementum surface cells. For the cementum surface cells there were significant ($P < 0.05$) differences between the regions. In every case the experimental tissue tested had higher readings than the controls (Figures 14a–c). Of particular interest in the bone surface cells was the increase in immunofluorescence labelling from the cervical to the apex in the controls and a reverse trend in the experimental teeth. This finding contrasted with the cementum surface cells, where the experimental teeth showed an increase from the cervical to the apical regions.

Observed data analysis for ET-1 background immunofluorescence in the PDL. Wald test for the effects of region and treatment on ET-1 immunofluorescence in the matching PDL background boxes, after removing the among tooth variance component, are shown in Table 4.

Significant ($P < 0.05$) interactions occurred between the treatment and region for ET-1 labelling in both the endothelium and bone background boxes. Little interaction occurred between the treatment and region for the cementum backgrounds. The treatment effect was significant ($P < 0.05$) for the cementum background boxes. In all but one case the background experimental values exceeded the controls. A very interesting trend was the decrease in immunofluorescence in the experimental teeth from the cervical to the apex.

Discussion

Control and experimental PDL endothelium revealed a punctate ET-1 cytoplasmic distribution

Table 3 Wald test for ET-1 upregulation: observed data.

Log of the ET-1	Wald statistic	d.f.	Endothelium	Bone	Cementum
Region		2	25.5*	21.3*	35.6*
Treatment		1	103.1*	223.5*	39.8*
Region by treatment		2	59.7*	101.8*	2.3

*$P < 0.05$.

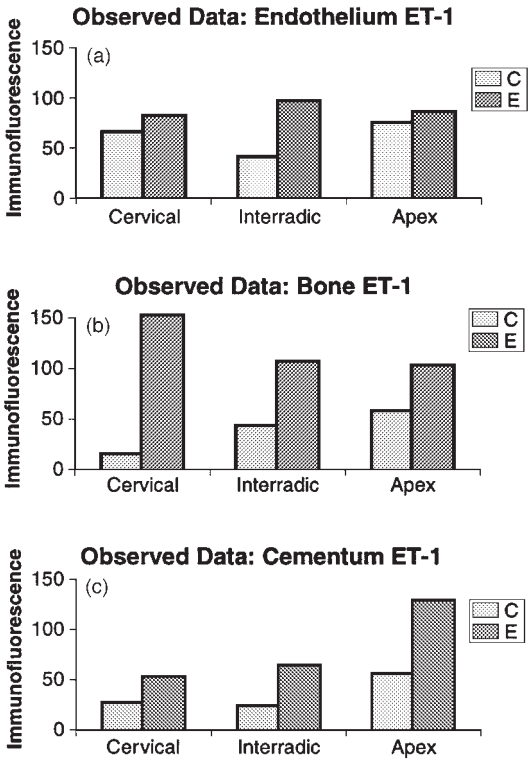

Figure 14 Observed data for (a) vessel endothelium, (b) bone socket surface and (c) cementum surface cell mean ET-1 immunofluorescence intensity levels from the analysis of the grey scale readings; 0–255 scale. C = control, E = experimental.

similar to that found in human embryonic kidney (Bhowmick *et al.,* 1998). The punctate expression of ET-1 within rat vessel endothelium raises the possibility that these arrays may indicate different stages of endothelin maturity or activity involving the autoregulation of PDL blood flow. There is a consensus opinion that ET-1 peptide can be produced locally in large amounts as an emergency and defensive response to inflammation, tissue damage, and wound repair (Properzi *et al.*, 1995; Webb, 1997) and that ET-1 synthesis may be related to the extent of endothelial activation (Vermes *et al.*, 1993).

The finding of ET-1 immunoreactivity in 40 per cent of PDL vasculature was not unlike that of Properzi *et al.* (1995) who reported that ET-1 was present in only 50 per cent of human cutaneous blood vessels. Their results could be explained by the fact that ET-1 is produced in a time-dependent manner and is said to reach equilibrium within a one hour generation period (Shima *et al.*, 1994). Regional variations in ET-1 immunoreactivity may also be due to diversity in the endothelin processing pathways within different vessel types (Gray, 1995). It can be concluded that the irregular pattern of ET-1 distribution in the rat MVB is determined by physiological and topographical micro-environmental variations created by normal

Table 4 Wald test for background ET-1 upregulation: observed data.

Log of the ET-1	Wald statistic	d.f.	Endothelium	Bone	Cementum
Region		2	90.7*	1.2	7.3
Treatment		1	123.4*	107.3*	42.3*
Region by treatment		2	103.9*	53.5*	5.7

*$P < 0.05$.

metabolic needs or experimentally-generated stress patterns. The doubling in the number of blood vessels identified in the loaded PDL suggests a rapid opening up of closed blood vessels akin to an hyperaemic or inflammatory response.

Specificity data for the rabbit anti-ET-1 antibody used in this study revealed cross-reactivity for ET-1 and big ET-1. Therefore, the present findings may also include some information for the ET-1 precursor, big ET-1 (Webb, 1997). Nevertheless, other projects including those of Barni *et al*. (1995), Horowitz *et al*. (1995), Wu and Tang (1998) have also used polyclonal ET-1 anti-sera from the same manufacturer for immunolabelling of endothelium.

The statistical analysis showed that despite the ratio data bias, there were clear, marked, and consistent differences between the experimental and control tissues. The Wald test is asymptotically distributed as a χ^2. However, due to the low number of degrees of freedom on which the test was based, the results should be interpreted conservatively. All tests of significance, except the ratio effect for ET-1 endothelium position ($P < 0.01$), gave probability levels of $P < 0.001$. Nevertheless, the overall analyses have been recorded at a conservative $P < 0.05$ level because of the limited number of animals from which the numerical data were collected. Although the values for the standard errors of the means (SEM) for the observed data were small, the SEM is sensitive to the statistical model chosen, and to have included them could potentially be misleading. Nevertheless, all five rats showed comparable immunofluorescence patterns with ET-1 and the findings highlight the potential for more extensive data studies.

From the ratio analysis, more ET-1 immunolabelling was present in the experimental sections and these differences were highly significant for endothelium, bone socket surface cells and cementum surface cells. The endothelium region by treatment interaction ($P < 0.05$) was due to a reversal of the effects between the apex and the other two regions. For the cementum surface cells, there was little interaction between the region by treatment. Nevertheless, there were significant ($P < 0.05$) differences between the cementum surface cell regions. These tissue and regional ratios (Table 2) become apparent when viewed as bar charts (Figure 13a–c).

Since the conventional method of ratio analysis (Tables 1 and 2; Figure 13a–c) introduced a background bias, the observed data were tested separately. From Tables 3 and 4, it proved necessary to consider the individual means for region and treatment effects, which demonstrate the distribution and upregulation of ET-1 immunofluorescence in the tissues examined (Figures 14 and 15).

In the endothelium of normal PDL, there was a higher level of ET-1 immunoreactivity than in bone and cementum (Figure 14a–c). Loading produced marked ET-1 labelling in all tissues, particularly the bone surface cells (Figure 14b).

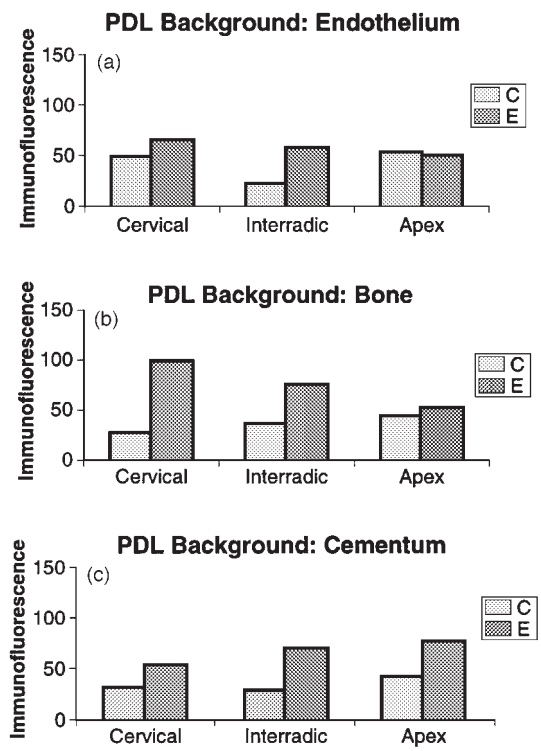

Figure 15 Observed data for background mean ET-1 immunofluorescence intensity levels for (a) vascular endothelium, (b) bone socket surface cells and (c) cementum surface cells in the PDL boxes; 0–255 scale. C = control, E = experimental.

The slope for the progressive cervical to apical ET-1 upregulation for bone surface cells was opposite to that found for the cementum surface cells (Figure 14c), where apical change predominated. These differences may reflect the variations in the response of these tissues, as well as the movement pattern of the root within the socket. Table 3 shows that there was little interaction between the treatment and region for the cementum surface cells. Therefore, the loading effect could be considered as acting more or less uniformly in all three cementum surface cell regions of the root. Figure 14a–c suggest that a relatively modest upregulation in ET-1 occurs in association with a substantial upregulation of ET-1 in bone and cementum surface cells, in particular. Just as ET-1 is known to participate in the regulation of bone resorption (Hierl *et al.*, 1998), it may also be a regulating component of cementum resorption. Since the cementum surface cells showed significant region differences ($P < 0.05$), the ET-1 immunofluorescence changes with loading may, therefore, provide a clue to the clinical sensitivity and resorptive potential of this tissue in some individuals from the early stages of orthodontic tooth movement (Harry and Sims, 1982).

Upregulation of ET-1 immunoreactivity in the PDL background (Figure 15a–c) also provides contrasting differences between and along the bone and cementum PDL surfaces. By comparison, endothelium ET-1 background values associated with the vessels were generally located more towards the middle of the ligament, showed intermediate values, and were more evenly distributed between the cervical and apical regions. These findings show that the PDL ET-1 background labelling responds to loading in a varying regional manner, like the endothelium, bone, and cementum. Thus, in terms of ET-1 distribution, microcirculatory function (Tang and Sims, 1992) and vessel morphology (Foong and Sims, 1999), the PDL is a complex heterogeneous structure.

The ET-1 distribution in the PDL invites further comparisons with investigations in other tissues. Stimulation of cultured endothelial cells is reported to take at least 30 minutes for the increased release of ET-1 (Yanagisawa *et al.*, 1988) and ET-1 is known to remain intact for up to 2 hours after cellular internalization (Bermek *et al.*, 1996; Bhowmick *et al.*, 1998). Thus, the present 3-hour experiment employing intact PDL extends the time span of other studies. It is also reported that plasma concentrations of ET-1 are known to increase more rapidly than could be attributable to *de novo* synthesis (Fyhrquist *et al.*, 1990) and, therefore, the store for rapid ET-1 release in the PDL may reside in endothelial secretory granules.

Apart from the mechanical stress generated by experimental loading, normal MVB physiology includes routine endothelial cell shear stresses that arise from viscous interactions between flowing blood and the endothelial wall (Pries *et al.*, 1995). Shear stress is reported to influence the release of ET-1 and the sparodic immunolabelling of ET-1 throughout the control PDL MVB may reflect locally different shear gradients generated by pulsatility and flow reversal (Skalak and Price, 1996). It is pertinent to emphasize that the rat tooth intrusional loading employed here was insufficient to produce vascular occlusion.

Pan-endothelial ET-1 labelling of vessels raises the question of vasoactivity propagation and vascular signalling mechanisms. Segal and Duling (1989) propose that propagation of locally initiated vasodilation/vasoconstriction response may be mediated by changes in membrane potential, spread electrotonically through gap junctions coupling smooth muscle cells, endothelial cells, or both. It is further suggested (Segal *et al.*, 1989) that the arteriolar network functions as a highly co-ordinated syncytium, with the result that diverse vasomotor stimuli can be summed and integrated within the peripheral vasculature. Thus, ET-1 effects in the endothelial tubes of the PCV, which lack smooth muscle, may give rise to distant vasomotor responses via electrotonic conduction to sites containing smooth muscle.

The distribution and upregulation of ET-1 labelling in the rat PDL invites further speculation regarding the likely distribution of ET_A and ET_B receptors in relation to vascular smooth muscle and endothelial cells within this tissue. It is

generally accepted (Webb, 1997) that smooth muscle located close to ET-1 containing endothelial cells exhibits ET_A and ET_B receptors. From other microvascular studies it is thought that the ET_A receptors predominate at the cell surface in vascular smooth muscle and mediate contraction, while ET_B receptors are mainly confined to vascular endothelium (Webb, 1997; Wu and Tang, 1998) where they modulate vasoconstriction in response to ET-1 through the release of endothelium derived vasodilators, including nitric oxide and prostacyclin (Verhaar *et al.*, 1998). All of these products are said to be synthesized in vascular endothelium and continually released, but not stored there (Ozaka *et al.*, 1997). The interactions between ET-1 and the endothelially derived relaxing factors are considered important for the control of vascular tone.

The fact that VC and PCV in the rat PDL are devoid of smooth muscle, suggests that these vessels function as endothelial tubes. However, their endothelium labels for ET-1. From knowledge of other vascular beds, it is hypothesized that this endothelium may be characterized by the presence of ET_B receptors (Webb, 1997).

The findings in the present study are consistent with the operation of a dual endothelial control system of PDL blood flow. It is proposed that, in vessels consisting of only an endothelial layer, flow may be distally regulated, presumably upstream at vessels with smooth muscle cells, by the relatively slow onset and sustained constrictor action of ET-1 (Bakker *et al*., 1997). This occurs particularly at branching sites, which interacts with the rapid, but short-lived, effects of endothelial derived relaxing factors (Gray, 1995). This system may be complemented by the vessels with smooth muscle cells providing a rapidly acting constriction response (Bakker *et al.*, 1997) to ET-1 released from their own endothelial lining cells. Support for a functional association between endothelin and vascular smooth muscle may be inferred from Figure 10 which illustrates PCV endothelium containing ET-1 closely opposed to smooth muscle cells of an adjacent arteriole. It is relevant to note that across species, more than 50 per cent of the PDL blood volume is contained in VC and PCV vessels, whereas the balance of the microvasculature has a smooth muscle cell component (Foong and Sims, 1999).

Numerous cell types display immunoreactivity to endothelins (Liu *et al.*, 1998; Davenport *et al.*, 1998). It is recognized that the vasculature plays an important role in bone remodelling under normal and pathological conditions, and that endothelins are among the local regulators of osteoblastic and osteoclastic functions (Sandy *et al.*, 1993; Hiruma *et al.*, 1998). Therefore, it is pertinent to note that ET-1 positive vessels were sometimes found in close proximity to upregulated bone surface cells, and cementum surface cells in presumed zones of PDL shear and compression.

Continual mechanical stretch of rat osteoblasts *in vitro* (Dolce *et al.*, 1996) causes deformation, which is a mitogenic signal producing gene induction 15 minutes after strain is applied, that reaches maximum levels after 1 hour. Such a response is much earlier than in the present project. Nevertheless, other data show PDL endothelial cell upregulation of RECA-1 surface protein immunoreactivity after 10 minutes of continuous loading (Sims, 1999).

To the author's knowledge, ET-1 upregulation in cementoblasts during a 3-hour intrusion load has not been reported previously. This finding shows that these cells undergo a significant biochemical response to short-term, continuous loading. Therefore, ET-1 may be an important peptide in cementum cell metabolism. As with bone surface reactivity, ET-1 upregulated blood vessels were also present in close proximity to sites of cementum upregulation of ET-1 (Vandevska-Radunovic *et al.*, 1997). Cementum has a similar morphology to bone, and exhibits resorption with different types of clinical loading (Owman-Moll *et al.*, 1995; Lu *et al*., 1999).

Conclusions

Continuous, short-term, dental loads initiate significant ET-1 distributional changes in the PDL vascular endothelium, bone surface cells and cementum surface cells. The statistical findings clearly show marked differences between control and loaded teeth. It would seem, therefore, that despite the fact that numerical data were

collected from only two rats, the treatment effects are real and not fortuitous. Since ET-1 is consistently present in normal rat PDL microvasculature, it is established that ET-1 quiescence is not the default state in this tissue. The hypothesis was confirmed.

Address for correspondence

Professor M. R. Sims
4 Willowood Drive
Urrbrae
South Australia 5064
Australia

Acknowledgements

The support and advice of Associate Professor B. J. Gannon is recorded with sincere appreciation. Dr C. Carati kindly aided with sectioning equipment. Dr P. Kolesik provided invaluable assistance with confocal imaging. Dr R. Correll graciously undertook the statistical analyses. This investigation was supported by the Australian Society of Orthodontists' Foundation for Research and Education.

References

Ames R S *et al.* 1999 Human urotensin-II is a potent vasoconstrictor and agonist for the orphan receptor GPR14. Nature 16: 282–286

Bakker E N T P, van der Linden P J W, Sipkema P 1997 Endothelin-1-induced constriction inhibits nitric-oxide-mediated dilation in isolated rat resistance arteries. Journal of Vascular Research 34: 418–424

Barni T *et al*. 1995 Identification and localization of endothelin-1 and its receptors in human fetal jaws. Developmental Biology 169: 373–377

Bermek H, Peng K-C, Angelova K, Ergul A, Puett D 1996 Endothelin degradation by vascular smooth muscle cells. Regulatory Peptides 66: 155–162

Bhowmick N, Narayan P, Puett D 1998 The endothelin subtype A receptor undergoes agonist- and antagonist-mediated internalization in the absence of signaling. Endocrinology 139: 3185–3192

Brooks D P 1997 Endothelin: The 'prime suspect' in kidney disease. News in Physiological Sciences 12: 83–89

Casasco A *et al.* 1992 Immunohistochemical evidence for the occurrence of endothelin in the vascular endothelium of normal and inflamed human dental pulp. Journal of Dental Research 71: 475–477

Davenport A P, Kuc R E, Plumpton C, Mockridge J W, Barker P J, Huskisson N S 1998 Endothelin-converting enzyme in human tissues. Histochemical Journal 30: 359–374

Dolce C, Kinniburgh A J, Dziak R 1996 Immediate early-gene induction in rat osteoblastic cells after mechanical deformation. Archives of Oral Biology 41: 1101–1108

Foong K W, Sims M R 1999 Blood volume in human bicuspid periodontal ligament determined by electron-microscopy. Archives of Oral Biology 44: 465–474

Fyhrquist F, Saijonmaa O, Metsarrine K, Tikkanen I, Rosenloff K, Tikkanen T 1990 Raised plasma endothelin-1 concentration following cold pressor test. Biochemical and Biophysical Research Communications 169: 217–221

Gilbert T M, Pashley D H, Anderson R W 1992 Response of pulpal blood flow to intra-arterial infusion of endothelin. Journal of Endodontics 18: 228–231

Gray G A 1995 Generation of endothelin; Molecular characterization of endothelin receptors. In: Gray G A, Webb D J (eds) Molecular biology and pharmacology of the endothelins. R G Landes Company, Austin, Texas, pp. 13–37, 39–58

Harry M R, Sims M R 1982 Root resorption in bicuspid intrusion. A scanning electron microscope study. Angle Orthodontist 52: 235–258

Hierl T, Borcsok I, Sommer U, Ziegler R, Kasperk C 1998 Regulation of interleukin-6 expression in human osteoblastic cells *in vitro*. Experimental & Clinical Endocrinology & Diabetes 106: 324–333

Hiruma Y *et al.* 1998 Endothelins inhibit the mineralization of osteoblastic MC3T3-E1 cells through the A-type endothelin receptor. American Journal of Physiology 275: R1099–R1105

Horowitz M J, Clarke M R, Kanbour-Shakir A, Amico J A 1995 Developmental expression and anatomical localization of endothelin-1 messenger ribonucleic acid and immunoreactivity in the rat placenta: a Northern analysis and immunohistochemistry study. Journal of Laboratory and Clinical Medicine 125: 713–718

Liu Y, Yamada H, Ochi J 1998 Immunocytochemical studies on endothelin in mast cells and macrophages in the rat gastrointestinal tract. Histochemistry and Cell Biology 109: 301–307

Lu L-H, Lee K, Imoto S, Kyomen S, Tanne K 1999 Histological and histochemical quantification of root resorption incident to the application of intrusive force to rat molars. European Journal of Orthodontics 21: 57–63

Ong A C M 1996 Surprising new roles for endothelins. British Medical Journal 312: 195–196

Owman-Moll P, Kurol J, Lundgren D 1995 Continuous versus interrupted continuous orthodontic force related to early tooth movement and root resorption. Angle Orthodontist 65: 395–402

Ozaka T, Doi Y, Kayashima K, Fujimoto S 1997 Weibel-Palade bodies as a storage site of calcitonin gene-related peptide and endothelin-1 in blood vessels of the rat carotid body. Anatomical Record 247: 388–394

Patterson H D, Thompson R 1971 Recovery of inter-block information when block sizes are unequal. Biometrika 58: 545–554

Payne R W *et al*. 1993 Genstat 5, Release 3. Reference Manual. Clarendon Press, Oxford

Pries A R, Secomb T W, Gaehtgens P 1995 Design principles of vascular beds. Circulation Research 77: 1017–1023

Properzi G *et al.* 1995 Early increase precedes a depletion of endothelin-1 but not of von Willebrand factor in cutaneous microvessels of diabetic patients. A quantitative immunohistochemical study. Journal of Pathology 175: 243–252

Sandy J R, Farndale R W, Meikle M C 1993 Recent advances in understanding mechanically induced bone remodeling and their relevance to orthodontic theory and practice. American Journal of Orthodontics and Dentofacial Orthopedics 103: 212–222

Segal S S, Duling B R 1989 Conduction of vasomotor responses in arterioles: a role for cell-to-cell coupling? American Journal of Physiology 256: H838–H845

Segal S S, Damon D N, Duling B R 1989 Propagation of vasomotor response coordinates arteriolar resistances. American Journal of Physiology 256: H832–H837

Shima H, Kawashima Y, Ohmori K, Sugiura M, Kawashima K 1994 Endothelin converting enzymes in guinea-pig lung membrane fractions: purifications and characterizations. Biochemistry and Molecular Biology International 34: 1227–1234

Shiohama Y, Sasaki T, Shibasaki Y 1995 Histological and immunohistochemical study of endothelin-1 localization in periodontal ligament during experimental tooth movement. Dentistry in Japan 32: 75–78

Sims M R 1999 Blood vessel response to pan-endothelium (RECA-1) antibody in normal and tooth loaded rat periodontal ligament. European Journal of Orthodontics 21: 469–479

Skalak T C, Price R J 1996 The role of mechanical stresses in microvascular remodeling. Microcirculation 3: 143–165

Tang M F P, Sims M R 1992 A TEM analysis of tissue channels in normal and orthodontically tensioned rat molar periodontal ligament. European Journal of Orthodontics 14: 433–444

Vandevska-Radunovic V, Kvinnsland S, Kvinnsland I H 1997 Effect of experimental tooth movement on nerve fibres immunoreactive to calcitonin gene related peptide, protein gene product 9.5, and blood vessel density and distribution in rats. European Journal of Orthodontics 19: 517–529

Verhaar M C *et al.* 1998 Endothelin-A receptor antagonist-mediated vasodilation is attenuated by inhibition of nitric oxide synthesis and by endothelin-B receptor blockade. Circulation 97: 752–756

Vermes I, Spooren P F M J, Kalsbeek-Batenburg E M 1993 In addition to von Willebrand factor and urinary albumin excretion, plasmin endothelin is an indicator of endothelial dysfunction in diabetes mellitus. Diabetologia 36: 472–473

Wang X *et al.* 1996 Expression of endothelin-1, endothelin-3, endothelin-converting enzyme-1, and endothelin-A and endothelin-B receptor mRNA after angioplasty-induced neointimal formation in the rat. Circulation Research 78: 322–328

Webb D J 1997 Endothelin: from molecule to man. British Journal of Clinical Pharmacology 44: 9–20

Wu S Q, Tang F 1998 Impaired paracrine effect of endothelin-1 on vascular smooth muscle in streptozotocin-diabetic rats. Cardiovascular Research 39: 651–656

Yanagisawa M *et al.* 1988 A novel potent vasoconstrictor peptide produced by vascular endothelial cells. Nature 332: 411–415

Copyright of European Journal of Orthodontics is the property of Oxford University Press / UK and its content may not be copied or emailed to multiple sites or posted to a listserv without the copyright holder's express written permission. However, users may print, download, or email articles for individual use.